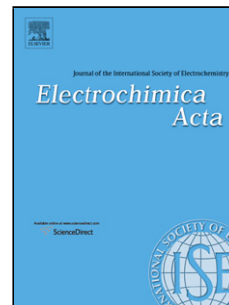


Accepted Manuscript

Title: Microwave-Assisted Synthesis of Pt-Au Nanoparticles with Enhanced Electrocatalytic Activity for the Oxidation of Formic Acid

Author: Gema Cabello Rogério A. Davoglio Fabian W. Hartl
Jose F. Marco Ernesto C. Pereira Sonia R. Biaggio Hamilton
Varela Angel Cuesta



PII: S0013-4686(16)32568-3
DOI: <http://dx.doi.org/doi:10.1016/j.electacta.2016.12.022>
Reference: EA 28494

To appear in: *Electrochimica Acta*

Received date: 13-10-2016
Revised date: 15-11-2016
Accepted date: 5-12-2016

Please cite this article as: Gema Cabello, Rogério A. Davoglio, Fabian W. Hartl, Jose F. Marco, Ernesto C. Pereira, Sonia R. Biaggio, Hamilton Varela, Angel Cuesta, Microwave-Assisted Synthesis of Pt-Au Nanoparticles with Enhanced Electrocatalytic Activity for the Oxidation of Formic Acid, *Electrochimica Acta* <http://dx.doi.org/10.1016/j.electacta.2016.12.022>

This is a PDF file of an unedited manuscript that has been accepted for publication. As a service to our customers we are providing this early version of the manuscript. The manuscript will undergo copyediting, typesetting, and review of the resulting proof before it is published in its final form. Please note that during the production process errors may be discovered which could affect the content, and all legal disclaimers that apply to the journal pertain.

Microwave-Assisted Synthesis of Pt-Au Nanoparticles with Enhanced Electrocatalytic Activity for the Oxidation of Formic Acid

Gema Cabello,^{*,1} Rogério A. Davoglio,^{*,1} Fabian W. Hartl,² Jose F. Marco,³ Ernesto C. Pereira,¹ Sonia R. Biaggio,¹ Hamilton Varela², Angel Cuesta⁴

¹ Departamento de Química, Universidade Federal de São Carlos, 13565-905, São Carlos, SP, Brazil

² Institute of Chemistry of Sao Carlos, University of Sao Paulo, POB 780, BR-13560970 Sao Carlos, SP, Brazil

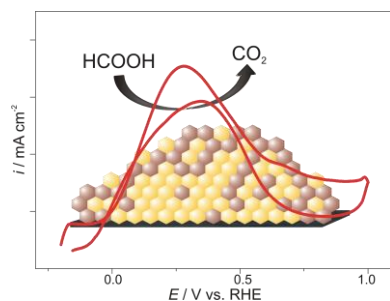
³ Instituto de Química-Física “Rocasolano”-CSIC, c/ Serrano, 119, 28006, Madrid, Spain

⁴ Department of Chemistry, School of Natural and Computing Sciences, University of Aberdeen, Aberdeen AB24 3UE, UK

*Corresponding authors: (GC) g.cabello@ufscar.br; (RAD) rogeriodavoglio@ufscar.br

(These authors contributed equally to this work).

Graphical Abstract



Abstract

We report the microwave-assisted hydrothermal synthesis of bimetallic Pt-Au nanoparticles with different Pt/Au mole ratio, and investigate their performance towards the electro-oxidation of formic acid. The as-synthesized Pt-Au sol was dispersed on a graphite electrode, without any binding agents, which allowed us to control the mass of alloy deposited. Pt-Au alloys showed better activity than bulk Pt and/or Pt nanoparticles towards the oxidation of formic acid, as evidenced by the decrease in the onset potential and the higher currents in the corresponding cyclic voltammograms. The higher activity is due both to atomic-ensemble effects, which lead the reaction through the so-called direct pathway with insignificant CO poisoning, and to electronic effects, which optimised the interaction between the catalyst surface and the reactive intermediate in the direct path. Further insight into the individual contributions of atomic-ensemble and electronic effects and their effect on the catalytic activity was provided by the analysis of galvanostatic potential oscillations.

Keywords

PtAu alloy; electrocatalysis; formic acid oxidation; microwave hydrothermal synthesis; potential oscillations

1. Introduction

Formic acid is an attractive fuel candidate for polymer electrolyte membrane fuel cells (PEMFCs) converting liquid fuel due, among other reasons, to its lower crossover diffusion through the membrane [1], and its better oxidation kinetics, and also because the onset potential for the formic acid oxidation reaction is lower compared to that of other C1 and C2 alcohols, such as methanol and ethanol [2]. Although Pt is very active towards the formic acid oxidation reaction (FAOR), it is susceptible of being strongly poisoned by intermediate reaction products, particularly CO, which has been traditionally explained by the so-called dual-path reaction

mechanism [3, 4]. For this reason, alloying of Pt with other metals has been attempted in order to improve its catalytic properties.

A second metal can promote several effects in Pt-bimetallic surfaces [5]. For instance, gold has been extensively used to influence the activity and selectivity of Group VIII metals due to its intrinsic stability [6-8]. Alloying changes the electronic structure of both metals in the alloy, as in the case of Group VIII metals combined with Group IB metals [9]. The resulting changes in the adsorption energy of reactants, intermediates and products may result in enhanced reaction rates, that can be electrochemically detected by an increase in the current density at low potentials [10]. Additionally, alloying can lead to, purely geometric, atomic-ensemble effects, that can channel the reaction through one of two or more possible pathways [11, 12]. For example, the alloying metal may disrupt sites composed of three contiguous Pt, which have been shown to be necessary for the dehydration of formic acid to adsorbed CO [13]. In principle, alloying will always give rise to both electronic and atomic-ensemble effects, although their weight in the final properties of the alloy will depend on the actual metal employed and on the atomic fraction of each material at the surface. However, it is difficult to obtain homogeneous and reproducible materials with traditional methods of synthesis.

The catalytic activity of bimetallic nanoparticles depends both on their composition and their structural properties, such as size, shape and morphology, which may be tuned via the synthesis method. Due to the potential technologic applications of nanoparticles, systematic studies of their physicochemical properties, both intrinsic (like, e.g., their atomic structure), and extrinsic (like, e.g., their size and porosity) are required. Classical methods of synthesis involve the reduction of metal precursor salts under heating conditions to promote the interdiffusion of the cations inside the metal lattice. These processes have slow rates and, consequently, long heating times are required. Processes which facilitate the synthesis of these materials by reducing the energy consumption and the reaction times are highly desirable. For instance, despite the high efficiencies obtained in the synthesis of Au [14-16] and Pt [17] nanomaterials by conventional methods, it is still necessary to optimize control over nucleation and growth, to impede agglomeration [18] (in order to obtain nanostructured materials with high surface area and good electrochemical properties), and to develop cleaner and more efficient processes according to the Green Chemistry Principle [19]. Among all modern methods of synthesis, the application of microwaves has attracted attention, due to easy handling and sample preparation, as well as to its diverse applications in organic synthesis, solid state reactions, and preparation of nanostructured materials [20-24]. The fundamental distinctive advantage of the application of microwaves to synthesis processes is linked to its high efficiency and low cost, since microwave energy is absorbed directly by the reactants instead of being absorbed by the vessel or reactor, like in conventional methods. Thus, uniform heating leads to more homogeneous nucleation and shorter crystallization times. Preparation of metastable phases not accessible by conventional methods of synthesis has also been reported, [25, 26] although microwave-specific thermal effects, as well as microwave non-thermal effects, are still a controversial matter. In this way, microwave-hydrothermal processes are gaining significance due to the feasibility of controlling the structure of the materials and the reaction selectivity by simply controlling temperature, reaction time and pressure. In consequence, this is a broad interdisciplinary field that is growing rapid and steadily.

This paper reports the synthesis, using microwave-assisted hydrothermal synthesis, of Pt-Au nano-alloys with high electrocatalytic activity for the FAOR.

2.1 Chemicals

All solutions were prepared using analytical grade reagents (purchased from Aldrich in the purest commercially available grade) and Milli-Q water (18.2 M Ω cm, Millipore). Solutions were degassed using nitrogen (99%, White Martins) and all measurements were carried out at room temperature.

2. Experimental

2.2 Instrumentation

All electrochemical experiments were performed with an Autolab PGSTAT302 electrochemical workstation (Eco Chemie) in a three-compartment electrochemical glass cell. The working electrode was a highly porous graphite electrode and the auxiliary electrode was a platinum wire. All potentials are reported versus the reversible hydrogen electrode (RHE). Synthesis of nanoparticles was performed in a microwave reactor Monowave 400 (Anton Paar). Scanning electron microscopy (SEM) images were obtained with a Supra-35 ZEISS FESEM system. Transmission electron microscopy with high resolution (HR-TEM) was performed with a Tecnai G2, FEI microscope. X-ray diffraction data were obtained using a Shimadzu diffractometer model XRD-6000, electrode voltage 30 kV, Cu K α radiation, in θ - 2θ mode, at 1° s⁻¹. XPS data from the nanoparticles and the corresponding electrodes were recorded with a nine channeltron Phoibos-150 hemispherical analyzer (specs) under a vacuum better than 1x10⁻⁹ mbar using Mg K α radiation and a constant pass energy of 20 eV. The binding energy scale was referenced to the C 1s signal of the adventitious carbon layer which was set at 284.6 eV.

2.3 Nanoparticles synthesis and working electrode preparation

Pt-Au nanoalloys were synthesized by chemical reduction of the precursor salts (hydrogen hexachloroplatinate (IV) hydrate (H₂PtCl₆·6H₂O) and hydrogen tetrachloroaurate (III) trihydrate (HAuCl₄·3H₂O)) with trisodium citrate dehydrate (Na₃C₆H₅O₇, TSC) under microwave radiation, controlling the [PtCl₆]²⁻ and [AuCl₄]⁻ ratios in order to obtain Pt, Pt₃Au, PtAu, PtAu₃ and PtAu₉ nanoparticles. All reagents were added to the microwave reactor, without any previous treatment, and were heated at 150°C for 6 minutes (10 bar). The obtained sol was centrifuged and washed several times with deionized water and dried at 60°C. 1 mg of the nanoparticles was dispersed in ethanol, dropped on the graphite electrode and dried at 100°C. The as-prepared electrodes were activated by cyclic voltammetry in 0.5 M H₂SO₄ until a *quasi* steady-state was reached. For the CO stripping measurements, CO was adsorbed at 0.3 V for 20 min and the adsorbed CO was oxidized at a scan rate of 20 mV s⁻¹ after eliminating the dissolved CO from the solution with N₂ for 30 min. Successive scans were carried out to verify the absence of CO in solution. The electrochemical active surface area (EASA) of platinum was calculated from the hydrogen adsorption/desorption charge assuming a charge of 210 μ C cm⁻² for a monolayer of adsorbed hydrogen, and compared with the charge of CO stripping, assuming a charge of 420 μ C cm⁻² for a monolayer of adsorbed CO.

3. Results and Discussion

3.1 Structural characterization: SEM, HR-TEM and XRD

Structural parameters are crucial in determining the reactivity of the nanoparticles, as they affect both electronic and geometric effects [5]. Therefore, a deep characterization of all these parameters may lead us to a better understanding of their catalytic performance. Electronic effects can be described based on the energy distribution of the d band density of states (DOS), and all other effects can be explained by geometric factors. We have performed SEM, HR-TEM

and XRD measurements in order to study the correlation between the lattice parameters and the electronic structure, as examined with XPS (see below), in these systems. Figure 1 shows the SEM (A-E), HR-TEM (F-J) and the selected-area electron diffraction (SAED) pattern for the Pt, Pt₃Au, PtAu, PtAu₃ and PtAu₉ nanoparticles, respectively. All samples (Figure 1 A-E) show small nanoparticles with similar size distributions. Clearly, aggregation of the nanoparticles increased with gold content. As shown by the HR-TEM images and the corresponding SAED patterns, all nanoparticles show hexagonal shape and high crystallinity, with predominantly (111) facets (inset), which we attribute to a combination of the experimental conditions and synthesis method employed. [27-29] The measured distances between two adjacent atomic rows for Pt nanoparticles was approximately 0.23 nm, which are characteristic of the separation between (111) planes of *fcc* Pt. Increasing the gold content led to an increase of defects. It was not possible to determine changes in the crystal lattice spacing related to the increase in the gold content, because the lattice parameters for platinum and gold (3.920 Å and 4.080 Å, respectively) are very close to each other.

The XRD pattern of the nanoparticles is shown in Figure S1. All XRD peaks could be indexed as face centered cubic (*fcc*) structure, and no peaks corresponding to other phases were detected. The sharp peaks indicate good crystallinity and the wide peaks, in combination with the HR-TEM analysis, could be attributed to small crystallite sizes. The average crystallite of the pure Pt nanoparticles was calculated from the peak width (FWHM) using Scherrer's equation, yielding an average size of 2 nm, in good agreement with the TEM analysis. Due to the limitations associated to the use of Scherrer's equation [30, 31] in bimetallic systems, we did not calculate the crystallite size for the PtAu alloys. We just can infer that the size of the nanoparticles slightly increased with the gold content as shown by the HR-TEM images. In the case of Pt NPs, the peaks at 2θ values 39.8°, 46.3°, 67.5°, 81.5° and 85.7° were attributed to the Pt (111), Pt (200), Pt (220), Pt (311), and Pt (222) planes of the *fcc* structure, respectively. Increasing the gold content in the nanoparticles led to a shift to lower angles of the corresponding peaks, which could be correlated to a good alloy formation. Peaks in the XRD pattern, compared to those of Pt, are shifted to lower 2θ as the bimetallic particles are formed. This can be indexed to an increase in the d-spacing crystal structure and expansion of the lattice constant as a result of incorporation of (larger) Au atoms into the Pt *fcc* lattice [32, 33]. The lattice constant values, calculated using Bragg's equation, for the different particles were 2.2749 Å (Pt); 2.3085 Å (Pt₃Au); 2.320 Å (PtAu); 2.3315 Å (PtAu₃) and 2.3432 Å (PtAu₉). These numbers fall between those of pure Pt and pure Au, confirming the formation of an alloy.

3.2 Chemical State Analysis from XPS and cyclic voltammetry

Surface composition of an alloy catalyst might be different to that of the bulk due to segregation. Thus, the chemical composition of the surface is an important parameter that will control at the end the reactivity of the catalyst. For this reason a deep surface characterization becomes necessary. Surface characterization of the particles was carried out by XPS and cyclic voltammetry.

Figure S2 shows the Au 4f and Pt 4f spectra recorded for each one of the materials considered in this paper. Because of the close vicinity of the Au 4f and Pt 4f spectral regions, the X-ray satellites corresponding to the Au 4f signal overlap with the Pt 4f_{5/2} core level peak. These

satellites were carefully subtracted from the spectra using software tools [34], otherwise the area of the Pt 4f peaks could be overestimated and therefore would lead to unrealistic Au/Pt atomic ratios. After satellite removal and background subtraction using the Shirley method [35], the spectral areas were obtained by peak integration and the Au/Pt atomic ratios calculated using the Multiquant XPS package software [36]. The results obtained are collected in Table 1. The data show that the Pt/Au atomic ratios are, in all cases, larger than the expected nominal values. This suggests that the surface of the nanoparticles is enriched in Pt. This enrichment appears to be larger for larger Pt contents. Inspection of Table 1 clearly shows that the binding energy of the Pt 4f_{7/2} core level decreases with increasing Au content in the electrodes (up to 0.7 eV from pure Pt to PtAu₉). This is an indication of the occurrence of Au-Pt alloying, which takes place at a greater extent for larger Au contents [37]. This must be the consequence of charge transfer between Pt and Au due to their different electronegativities [37-39], *i.e.*, of an electronic effect.

It is well-known that the Pt 4f and Au 4f core level peaks corresponding to platinum and gold metals are asymmetric, and that an exponential tail is required to adequately fit their corresponding spectra. In this paper we have fitted the Pt 4f and Au 4f core levels of pure Pt and Au metals using such an exponential tail, and the obtained value together with the rest of parameters, except the position and the area (line width, Lorentzian/Gaussian mixing ratio), have been fixed to fit the spectra of all the electrode series. This fitting procedure revealed the presence in PtAu₃ and PtAu₉ of a contribution with a binding energy around 72 eV, characteristic of Pt²⁺ (Table 1) [40], which could have been undetected/misestimated if all these parameters had been left to vary freely. The appearance of Pt²⁺ in gold-rich nanoparticles may be ascribed to a competition for the reducing agent, for which gold is expected to have higher affinity, during the synthesis procedure. Taken together, the XPS results suggest a situation in which the catalysts correspond either to a Pt-Au alloy covered by Pt islands or by a Pt-Au alloy completely covered by a thin Pt layer. In the terminology employed in ref [38] we would have a partially alloyed/partially phase segregated type of material. In some of the samples the outer part of the platinum islands/layer would be oxidized to Pt²⁺.

Figure 2 shows the voltammetric response of the graphite-supported Pt nanoparticles and the Pt-Au alloys, performed in aqueous 0.5 M H₂SO₄ solution. The currents were normalised to the Pt electrochemical active surface area (EASA), as calculated from the hydrogen adsorption/desorption charge. All graphs show the H_{upd}-region between 0 V and 0.4 V; the double layer region until oxide formation between 0.4 and 0.8 V, and the Pt oxide formation at $E > 0.8$ V, all of them typical voltammetric features of polycrystalline Pt. In addition, in Au-containing nanoparticles Au oxide formation occurs at $E > 1.25$ V. Oxide reduction peaks for Pt (peak I) and Au (peak II) appear during the reverse scan, exhibiting different intensities according to the Pt/Au mole ratio. In general, the CVs correspond to the weighted sum of those corresponding to pure Pt and pure Au surfaces, a clear evidence of the presence of both Pt and Au on the surface, although the platinum oxide reduction peak in Pt/Au alloys appears at slightly more negative potentials than in pure platinum. This is an indication of changes in the electronic structure of surface Pt, in good agreement with previous work [5, 8-10, 39, 41] and the XPS results above. The negative shift (in the order of 10-30 mV) of the platinum oxide reduction peak reveals a stronger bond between Pt and oxygen with increasing gold content. This can be attributed to a shift of the d-band centre to higher energies (closer to the Fermi level), leading to stronger bonding with adsorbates like oxygen or CO (see below). The potential of the gold oxide

reduction peak remained constant regardless of the Au content, again in good agreement with the absence of significant variations of the binding energy of the Au 4f_{7/2} XPS peak (see above).

3.3 CO stripping

The activity of an electrocatalyst towards the oxidation of methanol and/or formic acid is closely related to its tendency to form CO_{ads} and/or its ability to oxidise it once formed, both of which are influenced by both the surface composition and structure. Figure 3 shows the CO-stripping CVs of the different materials synthesised (current normalized to the EASA). Increasing the gold content in the alloy shifts the CO_{ads}-stripping peak positively. A similar behaviour has been previously reported, and explained by the existence of electronic interactions between Pt and Au [8, 10, 42]. Pedersen and co-authors calculated the chemisorption energy of CO on Pt-Au alloys as a function of the alloying degree and the d-band energy center [8] and found higher CO binding energy for lower Pt contents. This is consistent with the modification of the electronic structure of Pt upon alloying also suggested by XPS and the voltammetric characterization of the materials.

The platinum EASA was calculated from the CO stripping peak for comparison with that obtained from H_{ads} and similar values were obtained.

3.4 Catalytic Activity Towards the Electrooxidation of Formic Acid

3.4.1. Cyclic Voltammetry in HCOOH-containing acidic solutions

It has been previously reported that increasing the Au content in PtAu alloys leads to a decrease in the formic acid oxidation activity due to a diminution in available active Pt atoms, together with a negative shift of the onset potential due to less CO poisoning, attributed to atomic-ensemble effects [10, 43-45]. The effect of gold content on the catalytic activity of our materials for the FAOR was studied by cyclic voltammetry in solutions containing 0.05 M FA and 0.5 M H₂SO₄. The results are presented in Figure 4. The CV profile of pure Pt nanoparticles in the presence of formic acid is characteristic of the dual pathway mechanism [46]. The first anodic peak (peak I, ~0.65 V) in the positive-going scan corresponds to the direct oxidation of FA through the dehydrogenation pathway, and the second peak (peak II, ~0.95 V) results from the stripping of adsorbed CO (a catalytic poison) and the consequent increase in the rate of formic acid oxidation [46]. Anodic peaks in the negative-going scan appeared as a consequence of the reduction of surface oxides (~0.8 V and ~0.55 V), which provides active sites for formic acid oxidation. Increasing the amount of Au content in the alloy causes: (i) a negative shift of the onset potential of the FAO reaction; and (ii) an increase of the anodic peak corresponding to the FA oxidation via the dehydrogenation (direct) pathway, indicating that the dehydration (indirect) pathway is substantially suppressed.

Pt and Pt₃Au nanoparticles showed higher peak currents in the second oxidation peak of the positive-going scan than in the first one, implying a high degree of CO poisoning. Moreover, Pt and Pt₃Au nanoparticles showed large hysteresis between the anodic and cathodic sweeps, also a clear indication of CO poisoning. The peak current of the second peak in the positive-going scan decreased, and the hysteresis became less pronounced, with increasing gold content, both becoming almost negligible for PtAu₃. This is clear evidence of decreasing CO poisoning with increasing Au content, which would become negligible for a Pt/Au ratio 1:3. Taking into account the CO-stripping results reported above, this must be attributed to a gradual suppression with

increasing Au content of the formation of CO_{ads} on Pt, due to the associated gradual decrease in the number of atomic ensembles containing a minimum of three contiguous Pt atoms on the surface of the nanoparticles.

Table 2 lists the onset overpotential (η) for the different materials prepared, calculated as the potential at which the oxidation current exceeds by 5% the baseline current (labelled with * on the CV plot), and taking into account that the equilibrium potential for the oxidation of formic acid at the concentration used (0.05 M HCOOH) is 0.038 V vs. RHE. From pure Pt to PtAu₃ the overpotential decreases with increasing gold content by more than 200 mV, again suggesting a higher catalytic activity of these particles towards the FAOR. PtAu₃ nanoparticles also showed a higher activity for the direct path per surface Pt atom (*i.e.*, higher oxidation currents when normalized by the Pt EASA). Both the lower onset potential and the higher current density (EASA-normalized) for the direct path can be attributed to (i) a stronger interaction of surface Pt atoms at the surface of PtAu₃ with the intermediate in the direct path [47, 48], which decreases the potential at which the reactive intermediate starts adsorbing and brings the adsorption energy of this intermediate closer to the optimum for catalysis (an electronic effect); (ii) Pt-ensembles on PtAu₃ too small to adsorb H_{upd} , but big enough for the FAOR, since the FAOR may occur in a Pt-Au site but H_{upd} adsorption requires pure Pt sites surrounded by two or more Pt atoms [49] (an atomic-ensemble effect); and (iii) both. XPS, CV and CO-stripping voltammetry showed clear evidence of an electronic effect on the Pt atoms at the surface of the alloys, but the current results do not throw any light about possible additional contributions from atomic-ensemble effects to the observed higher activity of PtAu₃ for the direct path of the FAOR.

The catalytic performance of our materials per Pt mass towards the FAOR was found to be similar to that of other PtAu nanoparticles prepared by other methods [50].

Figure S3 shows the CVs corresponding to the oxidation of formic acid normalized to the mass of platinum for each electrode. Pt-mass normalized currents are smaller for Pt₃Au than for pure Pt nanoparticles, which can be attributed to the presence on the surface of this material of less active Au atoms. On the contrary, for PtAu and PtAu₃ nanoparticles the Pt-mass normalized current is clearly higher than in the case of pure Pt nanoparticles. The current normalized by the EASA is similar in pure Pt and PtAu₃ alloys, and smaller in the case of Pt₃Au and PtAu, as shown in Figure 4 and discussed above. Consequently, the higher Pt-mass normalized currents observed with PtAu and PtAu₃ must be largely due to a better utilization of the Pt atoms in the nanoparticles. This agrees with the XPS analysis above, which showed Pt surface segregation.

3.4.2. Galvanostatic oscillations during the FAOR

As in the case of most small organic molecules [51] the electro-oxidation of formic acid is known to undergo kinetic instabilities under some conditions [52, 53]. Understanding non-linear dynamics in these systems can provide meaningful mechanistic and/or kinetic information.

Figure 5 displays galvanostatic experiments using distinct applied currents. Previous galvanodynamic sweeps were used to normalize the oscillatory region, in order to ensure comparable conditions. In all cases, oscillations drift spontaneously until the limit cycle collides

with the fixed point corresponding to the oxygen evolution reaction, where the electrode potential would jump to very high values if a cut-off at 1.0 V were not applied.

Oscillations in the electro-oxidation of formic acid and other small organic molecules are generally attributed to the oscillating surface coverage of adsorbed species, like reactants, oxygenated species, poisoning intermediates and anions from the supporting electrolyte [54]. The applied current is sustained essentially by the electro-oxidation of formic acid through the dehydrogenation pathway [55] and, at the same time, CO_{ads} can be formed by dehydration of formic acid, blocking surface sites but not contributing to the total current. Due to this surface poisoning, the potential needs to increase in order to sustain the applied current, and it continues increasing until the formation of oxygenated species via water oxidation becomes possible. These oxygenated species, whose coverage increase with increasing potential, assist the oxidation of CO_{ads} via a Langmuir-Hinshelwood step, whose rate is itself also potential dependent, because it involves an electron transfer. This behaviour can be observed in the chronopotentiometric profile of the formic acid oxidation, especially on Pt bulk electrodes [52, 53].

Since the oscillations on the Pt NPs show a well-known profile and expectable parameters, we have used them as reference for comparison with the gold-alloyed nanoparticles. Figure 5 reveals the great impact of alloying with Au, shown in the increase of the amplitude and the decrease in the number of cycles with increasing gold content, until the complete absence of oscillations in PtAu_3 nanoparticles. General parameters, like frequency, amplitude and length of the oscillating region (S_{osc}), are highlighted in Table 3:

Interestingly, Pt and Pt_3Au nanoparticles sustain oscillations with very similar frequency and number of cycles. However, no induction period before the emergence of oscillations exists in the case of Pt_3Au , while in the case of Pt nanoparticles, the induction period until the first cycle is around 3000 s. PtAu nanoparticles showed a different behaviour, with oscillations starting after ~1500 s. The induction period is the time needed for the system to reach the proper configuration for the emergence of oscillations, and also carries some random aspects. Longer induction periods are associated to less susceptibility to generate oscillations.

On PtAu nanoparticles the lower potential limit is about 100 mV less positive than that for pure Pt and Pt_3Au catalysts, in good agreement with the lower onset overpotential observed in the corresponding CV (Figure 4). The absence of potential oscillations in the experimental conditions investigated for the PtAu_3 and PtAu_9 nanoparticles is clearly due to the absence of CO poisoning on these materials, and related to the increasing presence of gold.

The rate of potential change during an oscillation, dE/dt , calculated by differentiating one oscillation cycle from minimum to minimum, is shown as a function of the potential in Figure S4. dE/dt corresponds to the rate of deactivation (rising slope) and subsequent reactivation (decreasing slope) of the surface. At the lower potential limit the rate of deactivation is almost zero. In this potential region the observed deactivation must be due to the formation of CO_{ad} , and the low rate of surface poisoning observed is in good agreement with the well-known fact that, despite not involving any net electron transfer, HCOOH dehydration on Pt follows an electrochemical mechanism [56-58]. As a consequence, the rate of CO_{ad} formation is potential dependent and goes through a maximum [57-59]. The lower potential limit of the oscillation cycle is more positive than that at which the rate of dehydration of formic acid can be expected to be maximum, [58, 59] hence the low deactivation rate.

The slow increase in the potential required to sustain the applied current due to the slow surface poisoning by CO_{ads} will eventually lead to the formation of adsorbed oxygenated species and surface oxides, which are necessary for the oxidation of CO_{ads} , but also inactive in the direct path of formic acid oxidation. Initially, the latter effect dominates, and the rate of surface deactivation increases slowly with increasing potential until a maximum is reached, after which the rate of CO stripping significantly increases, and the rate of deactivation decreases again and becomes zero at the positive limit of the potential oscillation. At this point, CO stripping becomes dominant and dE/dt becomes negative. As the potential decreases, the rate of reduction of surface oxygenated species increases, and so does the rate of surface reactivation, until a maximum is reached, after which it decreases and becomes zero at the lower potential limit, when the cycle starts again. The increase in the oscillation amplitude with increasing proportion of Au is due to the shift to more negative and positive potentials of the Pt oxide reduction and the oxidation of adsorbed CO, respectively. Also to be noted is the shift to more positive potentials of the potential of fastest deactivation, and the increase of the magnitude of dE/dt with increasing Au content, the latter effect being more intense in the reactivation loop. Both effects are due to the slower rate of formation of CO_{ads} , and the resulting lower degree of CO poisoning, brought about by alloying Pt with Au. The spontaneous drift of the oscillations to more positive potentials, and their eventual fading, reflects surface deactivation [60-62] due to atomic place exchange at the catalyst surface as a consequence of platinum oxidation [46, 63].

The trends observed with increasing Au content in Pt/Au alloy nanoparticles are exactly the opposite to those observed in previous experiments on tin-modified platinum, in which the duration of the oscillations was considerably extended [64, 65], and the upper limit of the oscillations gradually decreased with time. Both observations were attributed to the fact that tin provides oxygenated species for the oxidation of adsorbed CO at lower potentials than platinum (bifunctional mechanism), preventing the oxidation and consequent deactivation of the latter. The results reported here are, hence, a clear indication that the improved catalytic activity of Pt/Au alloy nanoparticles is not due to a bifunctional mechanism (as was to be expected, as Au is the only metal which is more stable in its reduced than in its oxidised state).

A deep analysis of the oscillations provides further insight into the roles and consequences of both atomic-ensemble effects and electronic effects. On one side, increasing the amount of Au decreases the number of atomic ensembles on which HCOOH can be dehydrated to CO_{ads} , decreasing the rate (and extension) of CO poisoning. This explains both the wider potential range in which dE/dt is low with Pt_3Au and PtAu, and the faster reactivation of the surface on these nanoparticles (Figure S4). On the other side, increasing the amount of Au also shifts positively the potential at which CO is oxidized, as well as that at which Pt oxide is reduced, explaining the more positive potential at which the maximum dE/dt is reached with Pt_3Au and PtAu. This will also increase the degree of oxidation of Pt, which explains the faster vanishing of the oscillations with increasing gold content.

3.5 Stability tests

Fuel-cells must not only be active and efficient, but stable over prolonged use. The long-term performance of the nanoparticles was explored by chronopotentiometry at the current of the voltammetric anodic maximum for each electrode in 0.5 M H_2SO_4 + 0.05 HCOOH (Figure S5). The potential remained practically constant after 3 days for Pt and Pt_3Au and a decay of less than 100 mV was found in particles with higher gold content. There are no evidences of a decrease in activity due to surface poisoning or loss of material, revealing that the as-synthesized

nanoparticles are stable and graphite a suitable support for practical applications in direct formic acid fuel cells.

4. Conclusions

Bimetallic alloy nanoparticles with different Pt:Au molar ratios were synthesized by a microwave- assisted hydrothermal route, and investigated for the electrocatalytic oxidation of formic acid. Results obtained from *ex-situ* XPS, cyclic voltammetry and CO_{ads} stripping show a marked electronic interaction between Pt and Au. Oxidation of CO_{ads} on Pt-Au particles with high gold content was shifted positively over 200 mV. Higher oxidation currents for the direct path of the FAOR and lower onset potentials with increasing Au content were attributed to this electronic effect, which leads to an improved interaction between the intermediate in the direct path and the Pt atoms on the surface of the catalyst. On the other hand, the decrease in poisoning by adsorbed CO with increasing gold content is due to blocking of the dehydration of formic acid through an atomic-ensemble effect. Voltammetric experiments showed that PtAu₃ nanoparticles performed best for the FAOR at low overpotentials. Further insight into the role of electronic and atomic-ensemble effects in improving the catalytic activity of Pt/Au alloy nanoparticles was obtained from an analysis of kinetic instabilities. Galvanostatic potential oscillations emerge, in some cases after an induction period, on Pt, Pt₃Au and PtAu nanoparticles, but are absent on PtAu₃ and PtAu₉, confirming the absence of CO poisoning in the latter materials. Nanoparticles with equal amounts of Pt and Au show the highest dE/dt , indicating fast deactivation and reactivation processes. Atomic ensemble effects explain the wider potential range in which dE/dt is low for Pt₃Au and PtAu, as well as the faster reactivation of the surface, while electronic effects explain the more positive potential at which the maximum dE/dt is reached with Pt₃Au and PtAu, as compared with Pt. This shows the potential of analysing kinetic instabilities as a complementary approach in electrocatalysis research. All electrodes showed good catalytic performance for long periods of time, with no evidence of poisoning or mass loss.

Our results yield relevant information about the effect of both electronic and ensemble effects in the catalytic activity of Pt/Au nanoparticles and, therefore, towards the design of more efficient and durable electrocatalysts.

Acknowledgements

Conselho Nacional de Desenvolvimento Científico e Tecnológico (CNPq) is gratefully acknowledged for financial support under Research Project BJT-2014/400117/2014-2 and for the research support (HV: grant (#306151/2010-3). São Paulo Research Foundation (FAPESP) is also acknowledged for financial support (grants #2013/07296-2 and #2013/16930-7), and scholarship (FWH: grant #2014/08030-9). GC gratefully acknowledges R. Camargo for his collaboration in the acquisition of the HR-TEM images and for useful discussion and suggestions.

Associated Content

Supporting Information

XRD patterns of Pt and Pt-Au catalysts; Au 4f and Pt 4f XP spectra of the materials prepared; Cyclic voltammograms of Pt and Pt-Au NPs, recorded in 0.05 M HCOOH and 0.5 M H₂SO₄ (Pt

mass normalized); dE/dt vs. E graphs obtained from the galvanostatic chronopotentiometric data; chronopotentiometric measurements are presented in the Supporting Information.

References

- [1] X. Ji, K.T. Lee, R. Holden, L. Zhang, J. Zhang, G.A. Botton, M. Couillard, L.F. Nazar, Nanocrystalline intermetallics on mesoporous carbon for direct formic acid fuel cell anodes, *Nat Chem* 2 (2010) 286-293.
- [2] J. Willsau, J. Heitbaum, Analysis of adsorbed intermediates and determination of surface potential shifts by dems, *Electrochim. Acta* 31 (1986) 943-948.
- [3] A. Capon, R. Parson, The oxidation of formic acid at noble metal electrodes, *J. Electroanal. Chem. Interfacial Electrochem.* 44 (1973) 1-7.
- [4] A. Capon, R. Parsons, The oxidation of formic acid at noble metal electrodes Part III. Intermediates and mechanism on platinum electrodes, *J. Electroanal. Chem.* 45 (1973) 205-231.
- [5] J.K. Nørskov, T. Bligaard, A. Logadottir, S. Bahn, L.B. Hansen, M. Bollinger, H. Benggaard, B. Hammer, Z. Sljivancanin, M. Mavrikakis, Y. Xu, S. Dahl, C.J.H. Jacobsen, Universality in Heterogeneous Catalysis, *J. Catal.* 209 (2002) 275-278.
- [6] J. Schwank, Gold in bimetallic catalysts, *Gold Bulletin* 18 (1985) 2-10.
- [7] G.J. Hutchings, M. Haruta, A golden age of catalysis: A perspective, *Appl. Catal., A* 291 (2005) 2-5.
- [8] M.Ø. Pedersen, S. Helveg, A. Ruban, I. Stensgaard, E. Lægsgaard, J.K. Nørskov, F. Besenbacher, How a gold substrate can increase the reactivity of a Pt overlayer, *Surf. Sci.* 426 (1999) 395-409.
- [9] R. Woods, The surface composition of platinum-gold alloys, *Electrochim. Acta* 16 (1971) 655-658.
- [10] M.D. Obradović, A.V. Tripković, S.L. Gojković, The origin of high activity of Pt–Au surfaces in the formic acid oxidation, *Electrochim. Acta* 55 (2009) 204-209.
- [11] T. Iwasita, Methanol and CO electrooxidation, in: V. W., A. Lamm, H.A. Gasteiger (Eds.) *Handbook of Fuel Cells: Fundamentals, Technology, Applications*, John Wiley & Sons 2003.
- [12] A. Cuesta, Atomic Ensemble Effects in Electrocatalysis: The Site-Knockout Strategy, *ChemPhysChem* 12 (2011) 2375-2385.
- [13] A. Cuesta, M. Escudero, B. Lanova, H. Baltruschat, Cyclic Voltammetry, FTIRS, and DEMS Study of the Electrooxidation of Carbon Monoxide, Formic Acid, and Methanol on Cyanide-Modified Pt(111) Electrodes, *Langmuir* 25 (2009) 6500-6507.
- [14] M. Faraday, *Philos. Trans. R. Soc. Lond* 151 (1857) 183.
- [15] J. Turkevich, P.C. Stevenson, J. Hillier, A study of the nucleation and growth processes in the synthesis of colloidal gold, *Discussions of the Faraday Society* 11 (1951) 55-75.
- [16] G. Frens, Controlled Nucleation for the Regulation of the Particle Size in Monodisperse Gold Suspensions, *Nature* 241 (1973) 20-22.
- [17] J. Turkevich, R.S. Miner, L. Babenkova, Further studies on the synthesis of finely divided platinum, *J. Phys. Chem.* 90 (1986) 4765-4767.
- [18] A.D. Pomogailo, G.I. Dzhardimalieva, Reduction of Metal Ions in Polymer Matrices as a Condensation Method of Nanocomposite Synthesis, *Nanostructured Materials Preparation via Condensation Ways*, Springer Netherlands, Dordrecht, 2014, pp. 13-89.
- [19] P.T. Anastas, J.C. Warner, *Green Chemistry. Theory and Practice*, Oxford University Press 2000.
- [20] V.K. Saxena, C. U., Microwave Synthesis: a Physical Concept, in: U. Chandra (Ed.) *Microwave Heating*, InTech 2011.
- [21] S. Komarneni, Q. Li, K.M. Stefansson, R. Roy, Microwave-hydrothermal processing for synthesis of electroceramic powders, *J. Mater. Res.* 8 (1993) 3176-3183.
- [22] V. Polshettiwar, R.S. Varma, Green chemistry by nano-catalysis, *Green Chem.* 12 (2010) 743-754.
- [23] B.I. Kharisov, O.V. Kharissova, U. Ortiz Méndez, Microwave Hydrothermal and Solvothermal Processing of Materials and Compounds, in: W. Cao (Ed.) *The Development and Application of Microwave Heating* 2012.

- [24] I. Bilecka, M. Niederberger, Microwave chemistry for inorganic nanomaterials synthesis, *Nanoscale* 2 (2010) 1358-1374.
- [25] C.C. Landry, J. Lockwood, A.R. Barron, Synthesis of Chalcopyrite Semiconductors and Their Solid Solutions by Microwave Irradiation, *Chem. Mater.* 7 (1995) 699-706.
- [26] S. Komarneni, H. Katsuki, Nanophase materials by a novel microwave-hydrothermal process, *Pure Appl. Chem.* 74 (2002) 1537-1543.
- [27] B. Baruwati, M.N. Nadagouda, R.S. Varma, Bulk Synthesis of Monodisperse Ferrite Nanoparticles at Water–Organic Interfaces under Conventional and Microwave Hydrothermal Treatment and Their Surface Functionalization, *J. Phys. Chem. C* 112 (2008) 18399-18404.
- [28] V. Polshettiwar, B. Baruwati, R.S. Varma, Self-Assembly of Metal Oxides into Three-Dimensional Nanostructures: Synthesis and Application in Catalysis, *ACS Nano* 3 (2009) 728-736.
- [29] H.J. Kitchen, S.R. Vallance, J.L. Kennedy, N. Tapia-Ruiz, L. Carassiti, A. Harrison, A.G. Whittaker, T.D. Drysdale, S.W. Kingman, D.H. Gregory, Modern Microwave Methods in Solid-State Inorganic Materials Chemistry: From Fundamentals to Manufacturing, *Chem. Rev.* 114 (2014) 1170-1206.
- [30] B.E. Warren, B.L. Averbach, The Effect of Cold - Work Distortion on X - Ray Patterns, *J. Appl. Phys.* 21 (1950) 595-599.
- [31] B.E. Warren, X-Ray Diffraction, Dover Publications, New York, 1990.
- [32] J. Luo, M.M. Maye, V. Petkov, N.N. Kariuki, L. Wang, P. Njoki, D. Mott, Y. Lin, C.-J. Zhong, Phase Properties of Carbon-Supported Gold–Platinum Nanoparticles with Different Bimetallic Compositions, *Chem. Mater.* 17 (2005) 3086-3091.
- [33] B. Post, X-ray diffraction procedures for polycrystalline and amorphous materials. Harold P. Klug and Leroy E. Alexander, John Wiley & Sons, New York, 1974, pp. 960. \$37.50, *X-Ray Spectrom.* 4 (1975) A18-A18.
- [34] M. Wesemann, Plot, 2007.
- [35] D.A. Shirley, High-Resolution X-Ray Photoemission Spectrum of the Valence Bands of Gold, *Phys. Rev. B* 5 (1972) 4709-4714.
- [36] M. Mohai, XPS MultiQuant: multimodel XPS quantification software, *Surf. Interface Anal.* 36 (2004) 828-832.
- [37] S.D. Wolter, B. Brown, C.B. Parker, B.R. Stoner, J.T. Glass, The effect of gold on platinum oxidation in homogeneous Au–Pt electrocatalysts, *Appl. Surf. Sci.* 257 (2010) 1431-1436.
- [38] B.N. Wanjala, J. Luo, R. Loukrakpam, B. Fang, D. Mott, P.N. Njoki, M. Engelhard, H.R. Naslund, J.K. Wu, L. Wang, O. Malis, C.-J. Zhong, Nanoscale Alloying, Phase-Segregation, and Core–Shell Evolution of Gold–Platinum Nanoparticles and Their Electrocatalytic Effect on Oxygen Reduction Reaction, *Chem. Mater.* 22 (2010) 4282-4294.
- [39] E. Irissou, F. Laplante, S. Garbarino, M. Chaker, D. Guay, Structural and Electrochemical Characterization of Metastable PtAu Bulk and Surface Alloys Prepared by Crossed-Beam Pulsed Laser Deposition, *J. Phys. Chem. C* 114 (2010) 2192-2199.
- [40] S.M. Ureta-Zañartu, C. Yáñez, G. Reyes, R.J. Gancedo, F.J. Marco, Electrodeposited Pt-Ir electrodes: characterization and electrocatalytic activity for the reduction of the nitrate ion, *J. Solid State Electrochem.* 2 (1998) 191-197.
- [41] M.W. Breiter, Electrochemical Characterization of the Surface Composition of Heterogeneous Platinum–Gold Alloys, *J. Phys. Chem.* 69 (1965) 901-904.
- [42] S. Kumar, S. Zou, Electrooxidation of Carbon Monoxide and Methanol on Platinum-Overlayer-Coated Gold Nanoparticles: Effects of Film Thickness, *Langmuir* 23 (2007) 7365-7371.
- [43] N. Kristian, Y. Yan, X. Wang, Highly efficient submonolayer Pt-decorated Au nano-catalysts for formic acid oxidation, *Chem. Commun.* (2008) 353-355.
- [44] P. Rodriguez, Y. Kwon, M.T.M. Koper, The promoting effect of adsorbed carbon monoxide on the oxidation of alcohols on a gold catalyst, *Nat Chem* 4 (2012) 177-182.

- [45] J. Zhang, D.N. Oko, S. Garbarino, R. Imbeault, M. Chaker, A.C. Tavares, D. Guay, D. Ma, Preparation of PtAu Alloy Colloids by Laser Ablation in Solution and Their Characterization, *J. Phys. Chem. C* 116 (2012) 13413-13420.
- [46] G. Samjeské, A. Miki, S. Ye, M. Osawa, Mechanistic Study of Electrocatalytic Oxidation of Formic Acid at Platinum in Acidic Solution by Time-Resolved Surface-Enhanced Infrared Absorption Spectroscopy, *J. Phys. Chem. B* 110 (2006) 16559-16566.
- [47] E. Casado-Rivera, Z. Gál, A.C.D. Angelo, C. Lind, F.J. DiSalvo, H.D. Abruña, Electrocatalytic Oxidation of Formic Acid at an Ordered Intermetallic PtBi Surface, *ChemPhysChem* 4 (2003) 193-199.
- [48] E. Casado-Rivera, D.J. Volpe, L. Alden, C. Lind, C. Downie, T. Vázquez-Alvarez, A.C.D. Angelo, F.J. DiSalvo, H.D. Abruña, Electrocatalytic Activity of Ordered Intermetallic Phases for Fuel Cell Applications, *JACS* 126 (2004) 4043-4049.
- [49] F. Maroun, F. Ozanam, O.M. Magnussen, R.J. Behm, The Role of Atomic Ensembles in the Reactivity of Bimetallic Electrocatalysts, *Science* 293 (2001) 1811-1814.
- [50] D.N. Oko, J. Zhang, S. Garbarino, M. Chaker, D. Ma, A.C. Tavares, D. Guay, Formic acid electro-oxidation at PtAu alloyed nanoparticles synthesized by pulsed laser ablation in liquids, *J. Power Sources* 248 (2014) 273-282.
- [51] M. Hachkar, B. Beden, C. Lamy, Oscillating electrocatalytic systems, *J. Electroanal. Chem. Interfacial Electrochem.* 287 (1990) 81-98.
- [52] P. Strasser, M. Eiswirth, G. Ertl, Oscillatory instabilities during formic acid oxidation on Pt(100), Pt(110) and Pt(111) under potentiostatic control. II. Model calculations, *The Journal of Chemical Physics* 107 (1997) 991-1003.
- [53] P. Strasser, M. Lübke, F. Raspel, M. Eiswirth, G. Ertl, Oscillatory instabilities during formic acid oxidation on Pt(100), Pt(110) and Pt(111) under potentiostatic control. I. Experimental, *The Journal of Chemical Physics* 107 (1997) 979-990.
- [54] T.J. Schmidt, B.N. Grgur, N.M. Markovic, P.N. Ross Jr, Oscillatory behavior in the electrochemical oxidation of formic acid on Pt(100): rotation and temperature effects, *J. Electroanal. Chem.* 500 (2001) 36-43.
- [55] Y.X. Chen, S. Ye, M. Heinen, Z. Jusys, M. Osawa, R.J. Behm, Application of In-situ Attenuated Total Reflection-Fourier Transform Infrared Spectroscopy for the Understanding of Complex Reaction Mechanism and Kinetics: Formic Acid Oxidation on a Pt Film Electrode at Elevated Temperatures, *J. Phys. Chem. B* 110 (2006) 9534-9544.
- [56] A. Cuesta, G. Cabello, C. Gutierrez, M. Osawa, Adsorbed formate: the key intermediate in the oxidation of formic acid on platinum electrodes, *Phys. Chem. Chem. Phys.* 13 (2011) 20091-20095.
- [57] A. Cuesta, G. Cabello, M. Osawa, C. Gutiérrez, Mechanism of the Electrocatalytic Oxidation of Formic Acid on Metals, *ACS Catalysis* 2 (2012) 728-738.
- [58] V. Grozovski, V. Climent, E. Herrero, J.M. Feliu, Intrinsic activity and poisoning rate for HCOOH oxidation on platinum stepped surfaces, *Phys. Chem. Chem. Phys.* 12 (2010) 8822-8831.
- [59] V. Grozovski, V. Climent, E. Herrero, J.M. Feliu, Intrinsic Activity and Poisoning Rate for HCOOH Oxidation at Pt(100) and Vicinal Surfaces Containing Monoatomic (111) Steps, *ChemPhysChem* 10 (2009) 1922-1926.
- [60] H. Okamoto, N. Tanaka, M. Naito, Chaos in the Oxidation of Formaldehyde and/or Methanol, *J. Phys. Chem. A* 101 (1997) 8480-8488.
- [61] H. Okamoto, N. Tanaka, M. Naito, Chaotic and Periodic Potential Oscillations in Formaldehyde Oxidation, *J. Phys. Chem. A* 102 (1998) 7343-7352.
- [62] H. Okamoto, N. Tanaka, M. Naito, Intermittencies and Related Phenomena in the Oxidation of Formaldehyde at a Constant Current, *J. Phys. Chem. A* 102 (1998) 7353-7361.
- [63] H. Angerstein-Kozłowska, B.E. Conway, W.B.A. Sharp, The real condition of electrochemically oxidized platinum surfaces, *J. Electroanal. Chem. Interfacial Electrochem.* 43 (1973) 9-36.

- [64] N. Perini, E. Sitta, A.C.D. Angelo, H. Varela, Electrocatalytic activity under oscillatory regime: The electro-oxidation of formic acid on ordered Pt₃Sn intermetallic phase, *Catal. Commun.* 30 (2013) 23-26.
- [65] N. Perini, B.C. Batista, A.C.D. Angelo, I.R. Epstein, H. Varela, Long-Lasting Oscillations in the Electro-Oxidation of Formic Acid on PtSn Intermetallic Surfaces, *ChemPhysChem* 15 (2014) 1753-1760.

Figure Caption

Figure 1. (A-E) SEM images of Pt (A) and Pt/Au 3/1 (B), 1/1 (C), 1/3 (D) and 1/9 (E) nanoparticles; (F-J) HR-TEM images of Pt (F) and Pt/Au 3/1 (G), 1/1 (H), 1/3 (I) and 1/9 (J) nanoparticles. The corresponding SAED patterns are shown below each of the HR-TEM images.

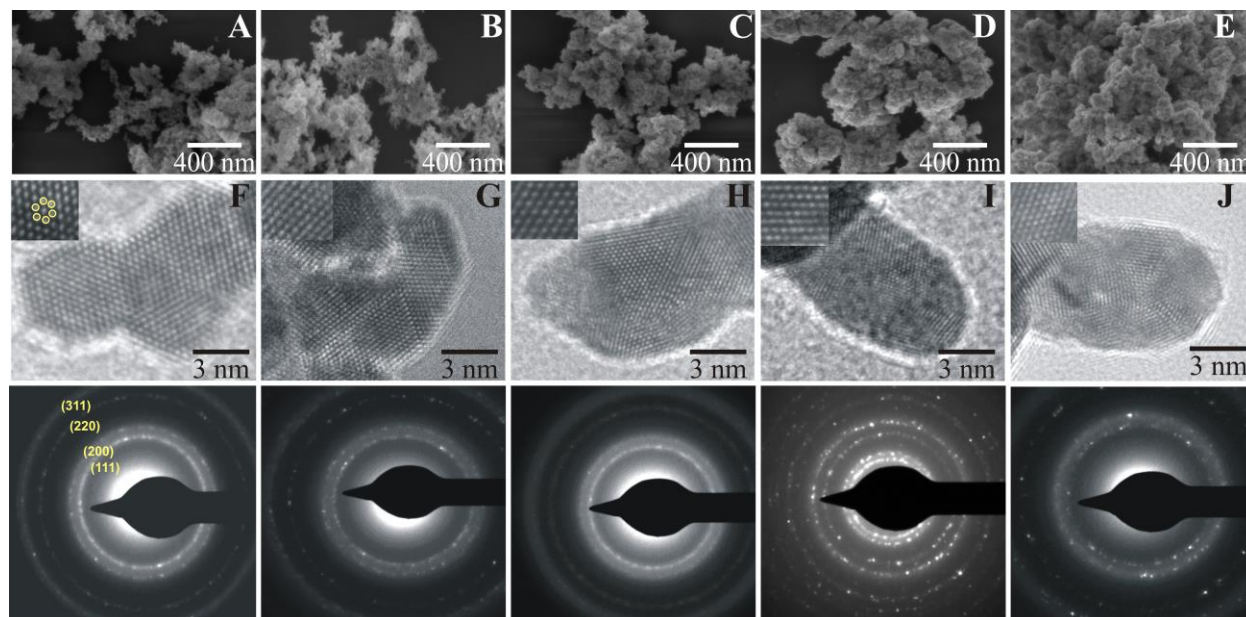


Figure 2. Cyclic voltammograms of graphite-supported catalysts, recorded in 0.5 M H₂SO₄ at 50 mV s⁻¹. Currents were normalized to the Pt electrochemical active surface area, as determined from the charge in the H_{upd} region.

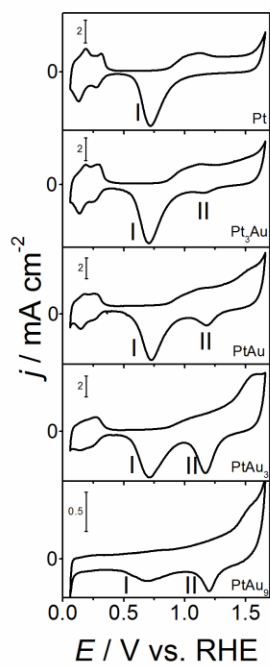


Figure 3. CO_{ads}-stripping voltammograms on Pt (black); Pt₃Au (red); PtAu (blue); PtAu₃ (green) and PtAu₉ (pink) electrodes in 0.5 M H₂SO₄, at 20 mV s⁻¹. Current densities are referred to the Pt EASA as obtained from the charge in the H_{upd} region.

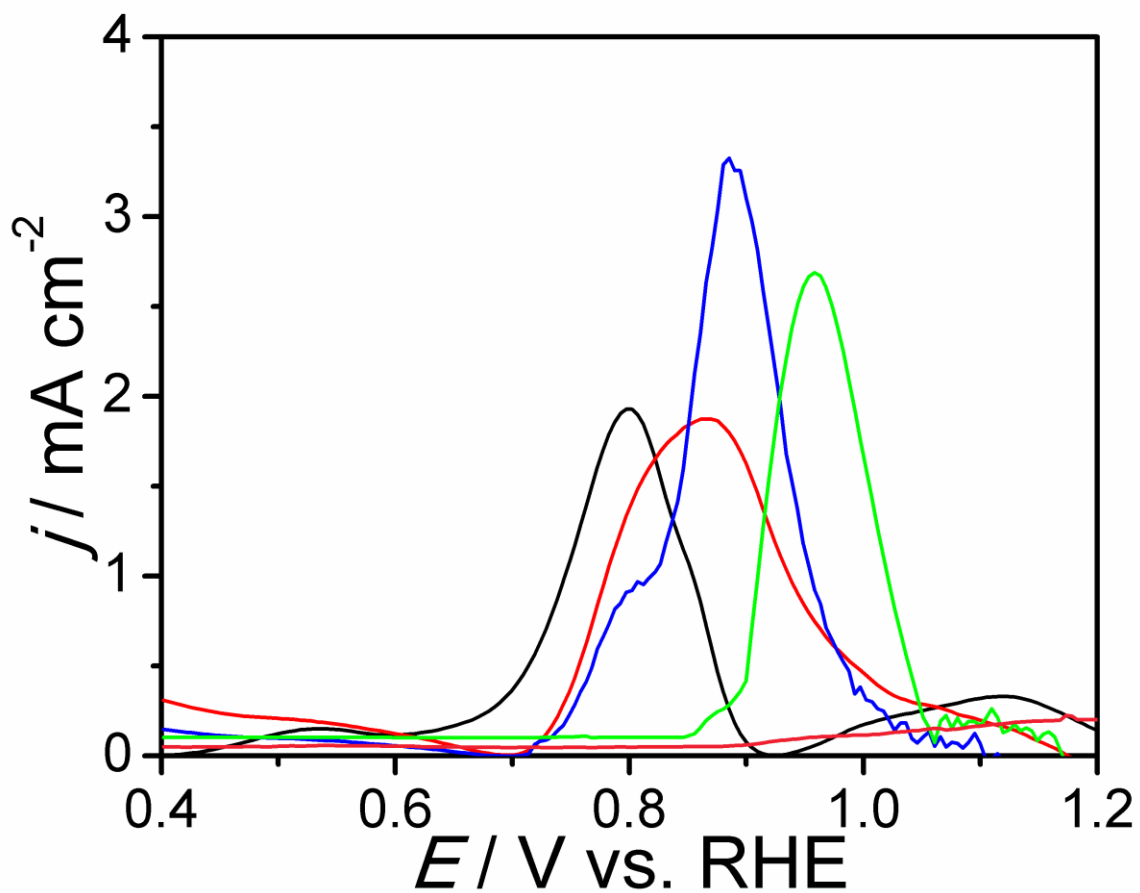


Figure 4. Cyclic voltammograms at 50 mV s^{-1} of Pt and Pt-Au nanoparticles supported on graphite in 0.05 M HCOOH and $0.5 \text{ M H}_2\text{SO}_4$. The figures in the upper right corner of the graphs indicate the Pt/Au ratio of the nanoparticles.

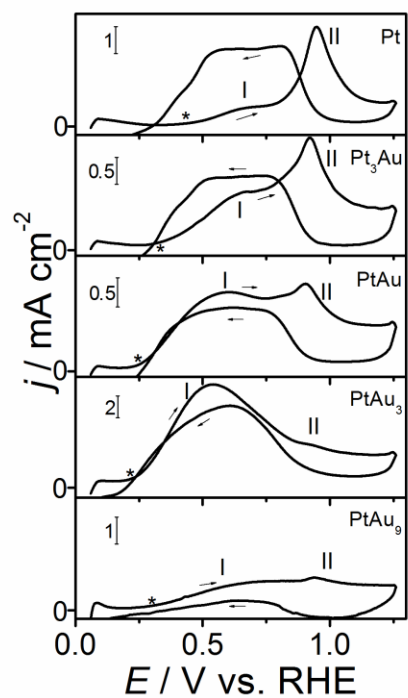
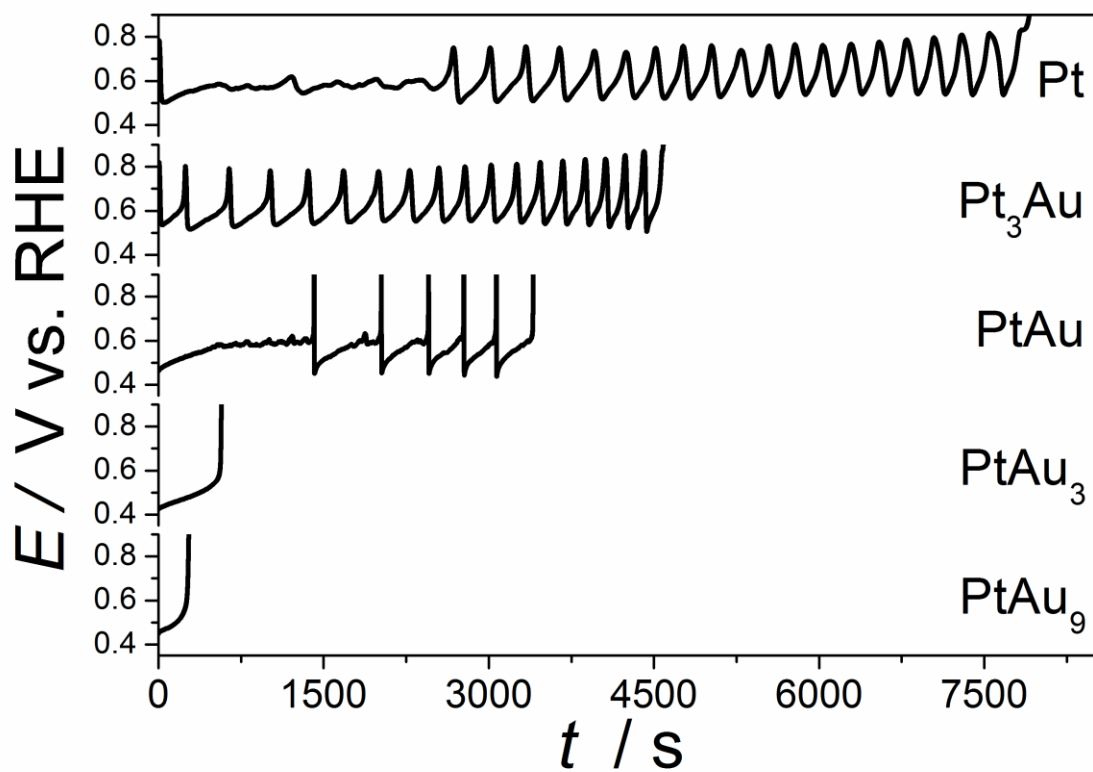


Figure 5. Potential time-series for the oxidation of formic acid on Pt (A), Pt₃Au (B); PtAu (C), PtAu₃ (D), and PtAu₉ (E) nanoparticles in 0.5 M H₂SO₄ + 0.2 M HCOOH. Applied currents: 3.9 mA (A); 4.3 mA (B); 12.8 mA (C); 2.7 mA (D); 1.5 mA (E).



	B.E. (eV) Pt 4f _{7/2}		B.E. (eV) Au 4f _{7/2}	Pt/Au atomic ratio
	Pt ⁰	Pt ²⁺		
Pt	71.6	-	-	-
Pt₃Au	71.5	-	84.1	5.56
PtAu	71.4	-	84.1	1.75
PtAu₃	71.3	72.6	84.2	0.39
PtAu₉	70.9	72.2	84.1	0.14

Table 1. Pt 4f_{7/2} and Au 4f_{7/2} binding energies of the different species found and Au/Pt atomic ratio obtained by XPS.

Pt/Au	1/0	3/1	1/1	1/3	1/9
$\eta / \text{V (RHE)}$	0.445	0.348	0.258	0.218	0.297

Table 2. Estimated values of the corrected onset-overpotential for all the electrodes (0.05 M HCOOH and 0.5 M H₂SO₄, 25°C).

Pt/Au	1/0	3/1	1/1	1/3	1/9
Amplitude (lower and upper limit of the oscillations) / V	0.27 (0.54-0.81)	0.32 (0.54-0.86)	0.43 (0.44-0.87)	-	-
Frequency / mHz	3.9	4.8	2.4	-	-
S _{osc} (S) / s	5200 (7900)	4600 (4600)	1700 (3400)	-(570)	-(270)
Number of Cycles	19	18	5	0	0
Min/Max dE/dt / mV s ⁻¹	-4.0/5.4	-8.3/22	-150/360	-	-

Table 3. Parameters of the oscillations reported in Figure 5. S_{osc} corresponds to the duration of the oscillatory region, and S is the time window for the whole evolution before the abrupt potential increase. dE/dt was obtained as the time derivative of the time series in Figure 5.